5-15-2009

In-situ Scanning Electron Microscopy for Electron-beam Lithography and In-situ One Dimensional Nano Materials Characterization

Renhai Long
University of New Orleans

In-situ Scanning Electron Microscopy for Electron-beam Lithography and *In-situ* One Dimensional Nano Materials Characterization

A Thesis

Submitted to the Graduate Faculty of the
University of New Orleans
in partial fulfillment of the
requirements for the degree of

Master of Science
in
Applied Physics

by

Renhai Long

B.S. Sichuan University, 2006

May 2009

Acknowledgement

This work was supported by the NSF Grant No. NSF-0403673, DARPA Grant No.HR0011-07-1-0032, and research grants from Louisiana Board of Regents Contract Nos. LEQSF(2007-12)-ENH-PKSFI-PRS-04 and LEQSF(2008-11)-RD-B-10.

I would like to express my gratitude to my advisor Dr. Weilie Zhou, who gave me the opportunity to study and research at UNO. I feel grateful for the discussion with Drs. John B. Wiley, Kevin Stokes, Leszek Malkinski and Leonard Spinu in AMRI meetings. Thanks are also given to Dr. Zhonglin Wang who cleared much of my confusion with the piezoelectric properties of the ZnO nanowire at 2009 AMRI-DAPAR Annual Review.

Speical thanks are given to Mr. Jiajun Chen, who trained me on all the facilities and help me a lot during my graduate study. Kai Wang, Yuan Yao and Jinhee Lim were very nice to prepare many high quality nanomaterials for my research. Research ideas and attitudes learned from Drs. Zhongming Zeng, Ying Li, Zengxing Zhang, Baobao Cao and Kun Yao are such great assets to me.

Finally, I extend my thanks to the faculty and the staff at both AMRI and the Department of Physics for their great care during my study at University of New Orleans.

Table of Contents

List of Figures

Abstract

In this thesis, we demonstrate *in-situ* scanning electron microscopy techniques for both electron beam lithography (EBL) and *in-situ* one dimensional nano materials electrical characterization. A precise voltage contrast image positioning for *in-situ* EBL to integrate nanowires into suspended structures for nanoswitch fabrication has been developed. The *in-situ* EBL eliminates the stage movement error and field stitching error by preventing any movements of the stage during the nanolithography process; hence, a high precision laser stage and alignment marks on the substrate are not needed, which simplifies the traditional EBL process. The ZnO piezoelectronics is also studied using nano-manipulators in scanning electron microscope. Methods to improve the contact have been demonstrated and the contacts between probe tips and the nanowires are found to have significant impact on the measurement results.

Keywords: electron beam lithography, voltage contrast imaging, piezoelectronics, nanowire, *in-situ*, ZnO.

Introduction

Electron microscopes are pivotal figures in the nano science and technology research. Since the date of their birth, the potential to study the dynamic process has been realized. A series of high resolution images actually can keep track of the gradual changes caused by deliberate actions. Over the years, *in-situ* electron microscopy has been developing fast with the thriving microelectronics industry, as more tools can be elegantly designed and micro-fabricated. The *in-situ* technology is being applied to both the existing research problems and new frontier of nano sciences.

In this work, we demonstrate the *in-situ* scanning electron microscope (SEM) techniques for both electron beam lithography (EBL) and *in-situ* one dimensional nano materials measurement. The chapters are organized as follows: Chapter 1 presents the overview of existing *in-situ* SEM tools and applications. Chapter 2 focus on the development of *in-situ* EBL through the fabrication of nanowire switches (One paper[2] on this work has been submitted for publication). Then, in Chapter 3, we describe how to do the *in-situ* SEM measurement on nanowires and study the ZnO piezoelectronics using nanomanipulators (This work[3] is under preparation for submission). Finally, in Chapter 4, we summarize our work on the *in-situ* SEM technology.

Chapter 1 Introduction to *in-situ* SEM

Researchers have long realized the potentials of the microscopes to study the dynamic process. Experiments where the specimens are acted on while they remain under continuous observation are *in-situ.* Generally in an *in-situ* experiment, specimens are modified in a deliberate way and the results are studied using the imaging and other analytical tools simultaneously.

In-situ technology in electron microscopy has been developing rapidly in recent years. Transmission electron microscopes (TEM) can now be armed with compactly-designed components for nanoindentation [4-7], straining and tensile tests [8-20], electrical characterization[21,22] and magnetic measurements[23,24] with the routine real time imaging. Specimen environment can be changed with heating and cooling, gas and liquid injection, materials deposition, etc.

As scanning electron microscope (SEM) is another important tool in the electron microscope lineup, the *in-situ* techniques are inspirational as well. The SEM specimen chamber is usually large enough to integrate lots of analytical tools, which are always challenging for TEM. Besides composition, morphology and structures, the magnetic, electrical and mechanical properties are also vital for application researches of nano materials, which is found to be marketable by some nano-positioning companies like Zyvex (http://www.zyvex.com), Nanotechnik (http://www.nanotechnik.com), 3rdTech (http://www.3rdtech.com) and so on. With the commercial tools and some customization, SEM can have versatile capabilities such as nanomanipulation, electron beam lithography (EBL), electrical probing, tensile measurement and so on.

The most common tools for *in-situ* SEM is the piezoelectric driven micromanipulators. Sharp probe tips with point radius down to tens of nanometers can be installed to the arms of the manipulators for sample manipulation and electrical probing. Many experiments can be carried out *in-situ.* For instance, by applying ac fields through the probe, excitation of nanowire resonance has been achieved and observed in SEM at real time[25]. However, for low level measurement special setup for noise shielding is essential as the electron beam and the manipulators themselves are major sources of the noise. Four-point probing is commonly carried out for low resistance measurement, where better manipulation skills or specific four-point measurement probe are required.

While loaded with force sensor, the micromanipulators are able to perform tensile and bending tests and monitor the response of the materials at the same time with high quality SEM imaging, which is a favorable technique for nano electromechanical system (NEMS) research and development. As microinjection tools are also available, tests of materials gas and bio sensing properties can also be realized *in-situ*. Even magnetic property testing[26] is possible with some calibrated homemade magnets inserted into the SEM chamber. Those *in-situ* SEM tool makers also discover potential market in electron beam lithography (EBL) by offering piezoelectric-driven, stable and precise stage as a competitive alternative to the high-end laser stages for dedicated EBL systems.

Though the *in-situ* SEM has a long history, a large body of *in-situ* SEM work is mechanical property related: fracture toughness and fatigue measurement [27-29], tensile deformation [30-35] and electromechanical study [31,36-38]. Such kind of experiments usually consists of an actuator for material deformation and load sensor for force read-out. Sometimes, the microscopes should be capable for the observation of the specimen

deformation and failure with very high resolution, while the load sensors are simultaneously measuring the applied load electronically with relatively high resolution. The specimen temperature can be controlled through the sample stage as well. Electrical probes will be used if electrical characterizations are needed. Such testing systems are an integration of electromechanical and thermomechanical components based on MEMS technology.

Huge variety of experiments has been made possible using *in-situ* SEM technology, given the convenience of integrating the required tools into the big SEM chamber. However the output data collected in *in-situ* experiments are more likely mixed with the artifacts than those *ex-situ* experiments. In the limited space of the chamber filled with various scientific instruments, signals are easily distorted with unknown noises. The recognition and elimination of artifacts should be given enough efforts both in the development of *in-situ* experiment tools and in the experiment methods.

Such an introduction to applications and tools of *in-situ* SEM is far from comprehensive and complete, as researchers are developing their ideas to make the existing tools more versatile and productive. Some disadvantages of the *in-situ* SEM today may be ingeniously solved tomorrow. The next chapter is a new capability we developed for *in-situ electron* microscopy. We use the *in-situ* SEM voltage contrast images to get rid of traditional EBL drawbacks for our nano device research.

Chapter 2 *In-situ* EBL for nano device fabrication

2.1 Overview of electron beam lithography

In microelectronic fabrication, dedicated electron beam lithography (EBL) systems can be used to either fabricate mask or directly write patterns on the wafer. Most direct write systems use a small electron beam spot that is moved with respect to the wafer to expose the pattern one pixel at a time. The systems can be classified as raster scan or vector scan with either fixed or variable beam geometries. All EBL systems need an electron source with high-intensity, high uniformity, small spot size, good stability and a long life. Electrons can be excited from cathode of the gun by heating the cathode (thermionic emission), applying a large electric field (field emission), a combination of the two (thermal field emission), or even with light (photoemission)[39]. As the pattern is transferred to the wafer sequentially one pixel at a time, the throughput is a major concern of EBL, especially when a raster scan system actually requires the beam to access each pixel. However, it is quite straightforward to use EBL to modify pattern and produce a small quantity of test units, since no mask making process is needed. The capability to make pattern at high resolution makes EBL an attractive technique for research and advanced prototyping, where throughput is not a major concern. By converting a scanning electron microscope, which has a very good electron source, a high resolution EBL system can be made at a small fraction of cost of a dedicated system.

Of the many custom designed SEM conversions, most use a set of digital-to-analog converters (DACs) to drive the scan coils of the microscope. The beam is modulated with a beam blanker. Alternatively, the beam can be blanked magnetically by biasing the gun alignment coils or not blanked at all. Lack of a beam blanker leads to the

additional problem of artifacts from the settling of scan coils and exposure at beam dump sites. Large patterns need to be split into multiple sub-fields for writing, and the sub-fields are then stitched together as the stage is moved over from field to field. Being designed for flexible imaging applications, SEM stages are neither flat nor homogeneously in focus during writing, and even when equipped with stepper motor control they are no more accurate than ~1 to 5 um[40]. Expensive high precision laser-controlled stage is available, but this is not a favorable option of many small research labs with tight budgets. Periodic alignment marks can be used to stitch fields accurately, but this requires extra processing as well as the use of photolithography for fabricating alignment marks. In order to make the alignment in a converted system as good as that of the dedicated one, the alignment mark should be at the center of the writing field due to large image distortion at the edge.

In summary, the inexpensive SEM EBL can provide adequate results for a number of applications like small number of transistors, small masks, test of resists, junctions, etc. Its practical applications are limited by stitching, alignment and automation. Due to the difficulties with stitching, SEM EBL is not practical for device integration over many fields. Multi-layer fabrication is challenging since much efforts need to be spent on alignment.

2.2 Electron beam lithography system at AMRI

The EBL at AMRI is performed by a Carl Zeiss LEO 1530VP SEM integrated with the nanometer pattern generation system (NPGS version: 9.0 SEM conversion kit sold by J.C. Nabity Lithography Systems). Figure 1 is the component graph of the whole system, and figure 2 is the real image of the whole system with the SEM on the left and NPGS PC on the right.

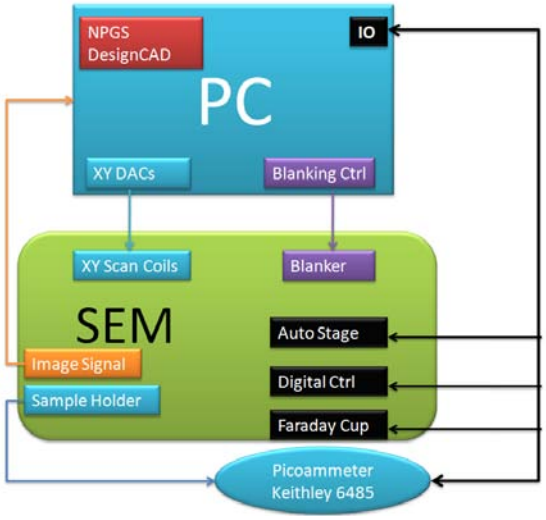

Figure 1 Component graph of electron beam lithography system at AMRI.

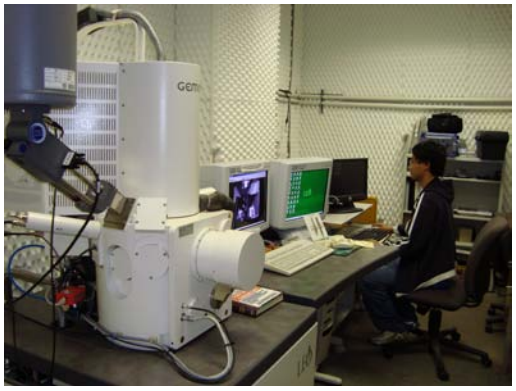

Figure 2 LEO 1530VP SEM and NPGS PC.

NPGS is built on a Windows PC with a PCI516 board (figure 3), which is used to generate the X and Y beam deflections and to provide the signals for blanking control in a Raith beam blanker controller (figure 4). The layout is designed using DesignCAD and converted to runfile by NPGS. To provide lower doses at reasonable currents, the Nabity system strobes the blanker at each exposure point. It also can monitor the beam current

Figure 3 PCI516 board of the NPGS at AMRI.

using Faraday cup on stage and a Keithley 6485 picoammeter, and adjust the dose during writing in case of an unstable beam. NPGS can control motorized stages, providing fully automated sample movement and pattern alignment.

Figure 4 Beam blanker controller.

Mark alignment on the NPGS is performed by calculating the correlation between the measured mark image and the user-defined mark pattern. Signal processing such as averaging and edge enhancement can be executed before the alignment correlation, allowing the use of low contrast or rough marks. If the user supplies precisely defined marks (usually printed with a mask made on a commercial mask making tool) then NPGS can be used to correct for global rotation, scaling, and nonorthogonality[40]. Typical alignment accuracies range from 1:1,000 of the writing field to ~1:5,000, with accuracies down to ~20 nm being possible[41].

2.3 Challenge for suspended nano-structure fabrication using nano materials

One-dimensional (1D) nanomaterials, such as nanowires, nanorods, and nanotubes, have been extensively studied for their applications in resonator[42,43], sensors and integrated circuits[44], etc. Lots of efforts have been put on the invention of standalone application-specific nanodevices[45], while some of others have been focused on the large scale integration of nanomaterials with traditional micro-electro-mechanical system (MEMS)[46]. In nanoelectromechanical system (NEMS), most structures require 1D nanomaterials move freely on a substrate, where a suspended structure is needed[47]. The most common way to fabricate a suspended nanowire structure is to etch away a sacrificial layer beneath the nanowire. In addition, the patterned electrodes must be precisely fabricated in a close proximity to achieve suspended nanomaterials structures. In the case of nanoswitches, it is necessary to fabricate a narrow gap to achieve controlled movements of suspended nanowires under electrical fields. A self-aligned split gate method had been developed to fabricate nano-size-spacing self-aligned side gates[1]; however, the spacing can hardly be controlled by changing the process parameters and the deposition materials of the electrodes for the sake of the yield. As shown in the figure 5, the self-align gate method was used to fabricate nano gap between electrode and the nanowire, however, only the right gaps got completely lift-off. The middle and the left electrodes still have some metals left in the bottom gaps. Moreover, the spacings between the electrodes and the nanowire are not identical even though they are made in the same batch.

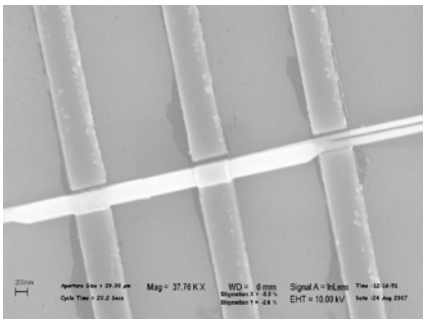

Figure 5 Self aligned gates fabricated using the method introduced in reference[1].

Integrating nano materials into suspended device structures was not an easy job due to poor alignment. Accurate alignment requires the fabrication of marks using photolithography and placing the mark at the center of the writing field, which sets lots of restrictions on the fabrication of nano devices using nano materials. Besides, the locations of the nanomaterials relative to the alignment mark need to be measured (figure 6) and registered before coating the photoresist for EBL. In figure 6, the target nanowire is measured to be located at (-7μm, 79μm) with respect to the alignment mark below. The

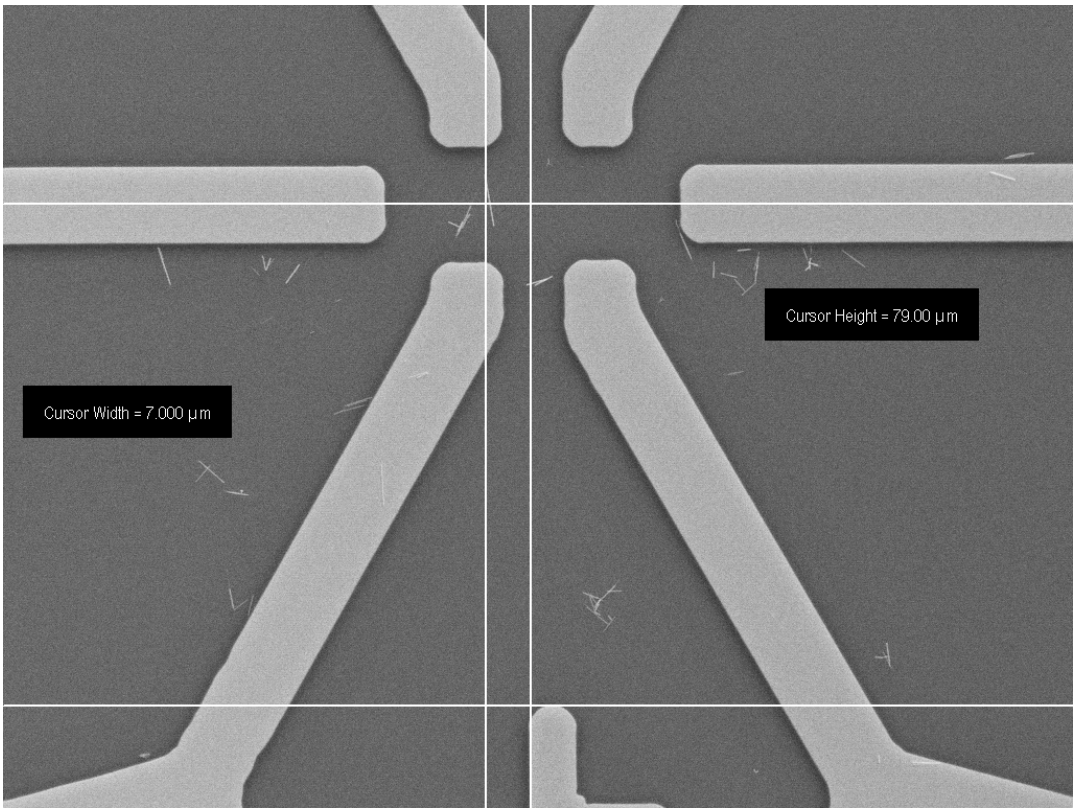

Figure 6 Measurement of the locations of the nanowire with respect to the alignment mark.

nanomaterials on the substrates were most likely to move during the spin coating of photoresist, which compromised the accuracy of the coordinates of the location. Once the

nanomaterials are far away from the alignment mark, there would be no chance to pattern accurately as the stage movement error had well exceeded the tolerance level of a pattern.

To tackle the problems as mentioned above, the *in-situ* EBL using one step process assisted by electron voltage-contrast imaging technique was developed for fabrication of electromechanical nanoswitches by suspending the nanowires and placing electrodes within controllable distance. The traditional EBL requires alignment to the alignment mark, which is not appropriate for the integration of nano materials into device structure fabrication. The *in-situ* EBL we developed aligns the pattern to the target nanomaterials, which is innovative in device fabrication process and application of *in-situ* electron microscopy. Such a technique can also be applied to integrate other suspended 1D nanomaterials in NEMS and MEMS fabrication.

2.4 Experimental details of *in-situ* EBL

The fabrication of the nanoswitches started from the *n*-type silicon wafer with 600 nm thick SiO_2 thermally grown on the top as shown in figure 7 (a). Big electrodes (figure 7 (b)) of 200 nm thickness were first fabricated by photolithography and metallic

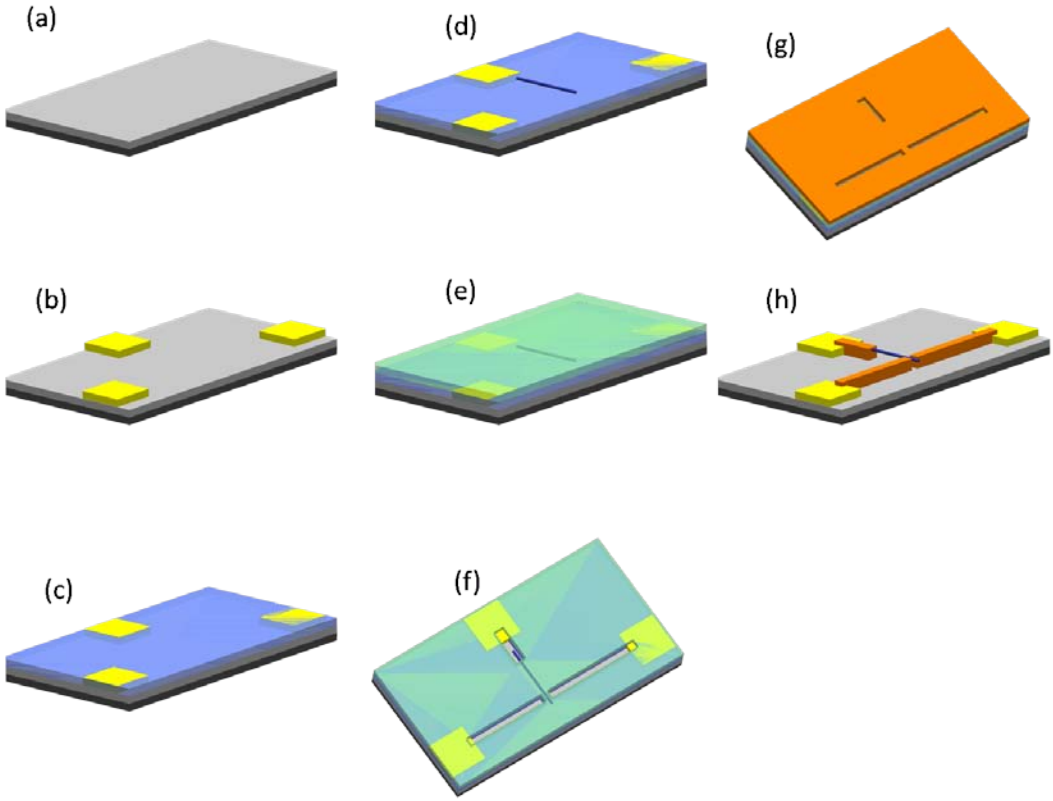

Figure 7 A schematic drawing of the fabrication process of a two-way switch. (a) Starting from an n-type silicon substrate with 600 nm thermal SiO_2. (b) Fabrication of big electrodes (200nm thick) using photolithography. (c) The first layer of photoresist (200nm thick) by spin-coating. (d) Dispersed nanowires on the photoresist. (e) A second layer of photoresist to sandwich the nanowires by spin-coating. (f) *In-situ* wrote and developed the pattern, and windows in photoresist are showed for metallization. (g) Deposited metal into the open windows; (h) the fabricated suspended nanoswitch after lift-off process.

deposition for easy measurement access. A layer of polymethylmetacrylate (PMMA) was then spin coated on the substrate to act as a sacrificial layer (light blue color in figure 7 (c)). The thickness of this layer defined the suspension height of the nanowires above the substrate. The nanowires, prepared using chemical vapor deposition or electrochemical deposition, were suspended in the isopropyl alcohol (IPA) solution. After 20 seconds of ultra-sonication, the nanowire solution was then dropped onto the substrate, followed by an immediate spin and oven bake (80^{o}C) to ensure the nanowires evenly dispersed (figure 7 (d)). A second layer of PMMA was then spin coated (light green in figure 7 (e)) so that the nanowires could be sandwiched in between. The locations of the nanowires were registered under scanning electron microscope using high magnification (10,000X) voltage contrast imaging technique. Direct *in-situ e*-beam writing was carried out to make the contact electrode and the deflection electrode with designed narrow gap. The exposed area of the PMMA was developed (figure 7 (f)) with a 1:3 mixture of methylisobutylketone (MiBK) and IPA, and gold (400nm thick) was sputtered (figure 7 (g)), followed by a lift off process to fabricate the whole structure (figure 7(h)). It should be noted that only one *e*-beam nanolithography and one lift-off process were needed to achieve the nanoswitch structure. The *e*-beam nanolithography was performed using Carl Zeiss 1530 VP field emission scanning electron microscope (FESEM) integrated with JC Nabity nanometer pattern generation system without high-precision stage. The pattern procedure is detailed as follows: (1) adjust the microscope to get the best imaging conditions at 10 kV at magnification larger than 10,000X (Smaller kV can be used to get better image contrast of the substrate and avoid unnecessary exposure of photo-resist), (2) keep the sample stage flat and move the beam to the dumped part of the substrate to adjust the focus, (3) store the imaging condition and get a low magnification (500 X ~

1,000 X) of the area of interest at 4 kV, (4) center the target nanowire to the center of the beam using image centering tab and restore the imaging condition at 10 kV, and then select a higher magnification (10,000 X) and catch the voltage contrast image of the target nanowire within 1 second, (5) use the previous stored high magnification image (in step 4) for device layout design and perform direct *in-situ e*-beam writing. The writing center of the layout should be exactly at the center of the image. It should be noted that the scanning must be stopped immediately after each image catch. The actual field area of the image can be precisely read by SEM software, as shown in figure 8, in which the actual area is 27.057 μm by 20.293 μm for this 10,000X image at aperture size of 20μm and working distance (WD) at 7 mm. The *in-situ e*-beam nanolithography mainly counts on the quality of the voltage contrast image and the precision of the field area to minimize the positioning error, since we cannot control the small vibration of the stage and the electron beam drift. The *in-situ e*-beam nanolithography eliminates the stage movement error by preventing any movements of the stage during the nanolithography; hence, a high precision laser stage is not needed. The fabrication of alignment marks on the substrate is also not necessary, which simplifies the traditional lithography process.

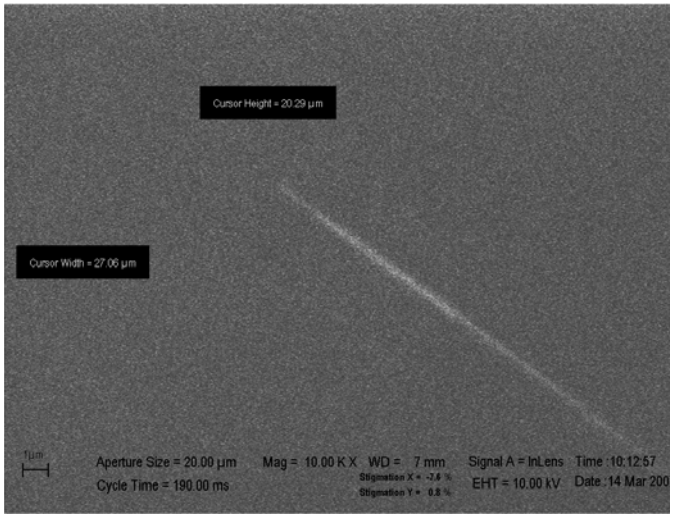

Figure 8 Clear voltage contrast image of a ZnO nanowire sandwiched between two layers of PMMA. The actual field area of this image is 27.057 μm by 20.293 μm, the scanning time is 190 ms, and the scale bar is 1 μm.

In a traditional way, aligning electrodes and making contacts to nanowires need registrations of the positions of the nanowires relative to the alignment marks. The coordinates of the nanowires are used to pattern contacts to the nanowires using *e*-beam nanolithography. Generally the alignment marks are at the corners of the die, and the target nanowires are far away at the center. The *e*-beam nanolithography requires the movement of the stages, so that the electron beam can be centered on the area of interest. The positioning accuracy can often be jeopardized by ordinary SEM stages movement accuracy. The accuracy can be better (<0.1 um) when converted SEMs equipped with the expensive high precision laser stages are used. Currently the commercially available dedicated *e*-beam nanolithography system, such as JEOL JBX-9300FS, has an overlay and stitching accuracy of 20 nm and positional accuracy of 25 nm[48]. However, such accurate results can barely be achieved in most research facilities where *e*-beam nanolithography is performed through converted electron microscope systems at a small fraction of the cost of a dedicated system. However, the positioning error in our method can be minimized to about 10 nm, which is already superior to most of the converted SEMs equipped with laser stages and can be widely used in nanodevice fabrication in converted SEM *e*-beam nano-writing systems.

2.4.1 Voltage-contrast imaging for EBL

The contrast mechanism in scanning electron microscope has long been studied[49]. By making use of the local potential differences between semiconducting nano-materials and the insulator substrate, a rapid imaging technique for nanotubes[50]was developed. Moreover, an alignment system using voltage contrast images was proposed by Nakasugi *et al*.[51]for low-energy *e*-beam lithography, which provides the advantages of high sensitivity, reduced charging, and low proximity and heating effects. To overcome the disadvantage of short penetration range of electrons in low energy *e*-beam nanolithography, many thin film techniques for photoresists were developed [52]. Since the deposited electrodes should be thick enough to clamp and suspend nanowires, we would like to take advantage of the rapid voltage contrast imaging technique for nanowire position registration and avoid the draw back from short penetration of the low energy *e*-beam nanolithography at the same time.

In our experiment, we tried to implement this idea in two ways: (i) Use low kV for imaging and high kV for e-beam lithography, (ii) Use mid-level kV for both imaging and *e*-beam lithography. The first way was unsuccessful because it was hard to find a precise image field and working distance matching between low kV imaging and high kV imaging, which resulted in poor alignment and resolution in *e*-beam nanolithography. The second approach led to a little bit poor voltage contrast image as the recommended voltage contrast imaging conditions are in the incident energy range of 2keV to 4keV[53]. However, by shortening the scanning time, an acceptable image was achieved without extensive exposure of the photoresist (PMMA).

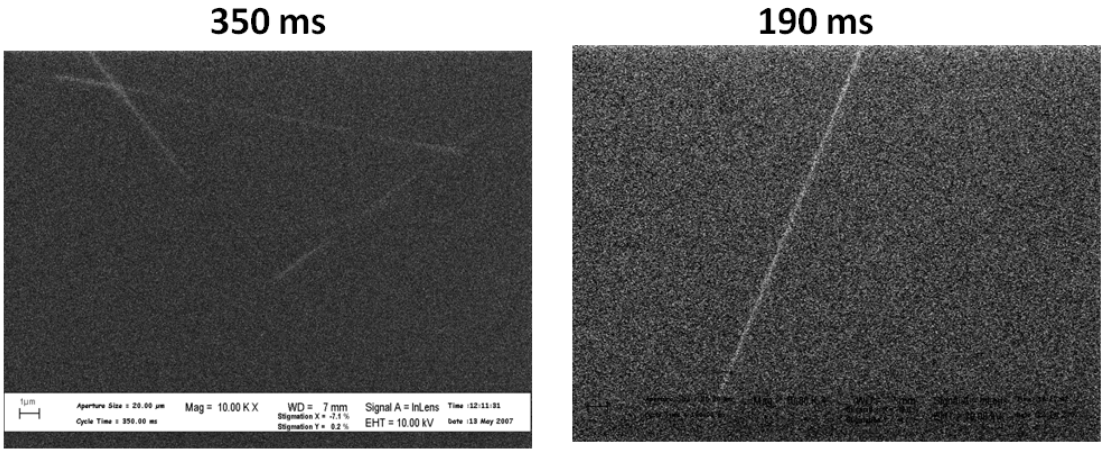

Figure 9 Contrast difference of the images captured with scan time of 350 ms and 190 ms.

In figure 9, images from left to right were taken at different scanning times of 350 ms, and 190 ms respectively. All other imaging conditions were kept the same. Evidently, the less the scanning time is, the better the contrast is. Edge and contrast enhancement on the image can improve the positioning accuracy as well. Here is an explanation of such phenomenon. During imaging, the electron beam bombards on the insulating PMMA surface, then the PMMA is negatively charged[54]. In this case, the semiconducting nanowires are positive with respect to the PMMA. Differences in surface electrostatic potential affect the number of secondary electrons leaving the PMMA. A positive surface will increase the secondaries, while a negative surface will decrease the number of secondary electrons. If longer time is taken, the whole image field will tend to be potential equilibrium, which lowers the contrast. That's why shorter scanning time would help us get better contrast.

As the area of interest had been previously exposed for imaging in a short time, the lower dose than normal was needed to avoid over exposure. Meanwhile, the stage should

be kept still right from the last imaging till the end of direct writing to achieve better alignment, which is comparable to the results of a dedicated *e*-beam system.

2.4.2 Layout editing for positioning accuracy optimization

Layout editing for EBL is a little bit tricky for positioning accuracy optimization. Before, users of EBL liked to set the lower left corner of the pattern as the origin of the pattern, this would results in poor positioning due to image distortion at the edge of the writing field. What's worse, even with beam blanker, the LEO 1530 VP scanning electron microscope tends to dump the beam to the lower left corner of the writing field now and then (figure 10).

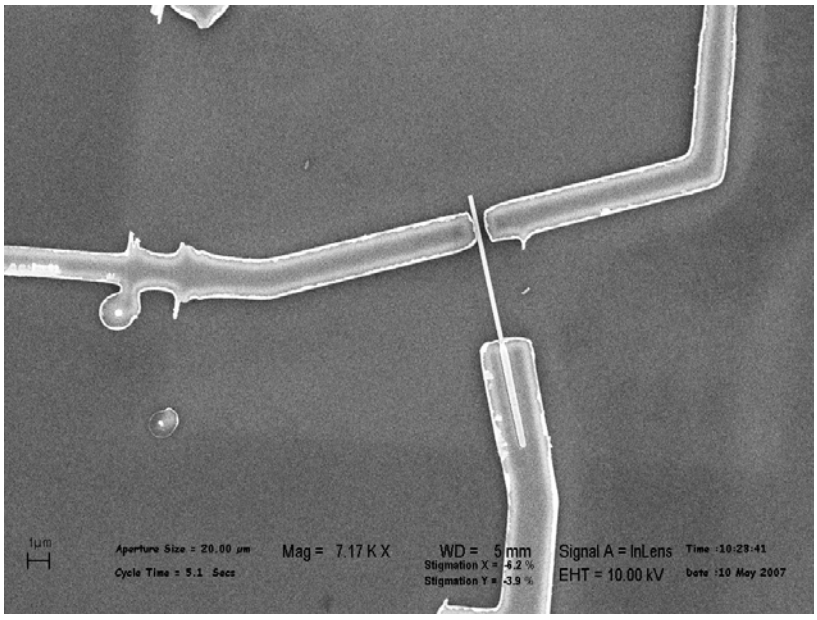

Figure 10 Small balls formed on the lower left corner due to the beam dumping, which cannot be avoided in our system.

Setting the origin to the center of the voltage contrast image is highly recommended. To set the origin to the centre of the image, the accurate filed size of the image must first be set. For a typical 10,000 X magnification image, the filed size is 27.057 µm by 20.293 µm. Then the lower left corner of the image is set to (0,0), so that the upper right corner corresponds to (27.057, 20.293). Now the center of the image is (13.528, 10.147),

which needs to be set as the origin. Without these correct coordinates information, precise alignment or positioning can barely be achieved. Another advantage of setting the origin to the center of the image is that higher writing magnification can be set in the run file. The NPGS support up to 10,000 X writing magnification. The higher the writing magnification, the better the writing feature and alignment. Besides, if the writing magnification is not kept the same as that of imaging magnification, the center of the field would change a little because of magnification change. The NPGS might not be able to correct this change; hence, the accuracy would be undermined.

2.4.3 Proximity effect

Due to the electron scattering, the dose delivered by the electron beam is not confined to the shapes that are supposed to be exposed, which results in line-width variations. If two pattern features are very close to each other, significant unintentional exposure or proximity effect would damage the whole pattern (figure 11). In our fabrication of nanoswitches, the proximity effect usually ruined the patterns as the designed face-to-face electrodes are less than 500 nm apart. A number of algorithms have been developed that can be used to compensate for proximity effect. Generally these algorithms calculate the concentration of surrounding features suitably weighted by their

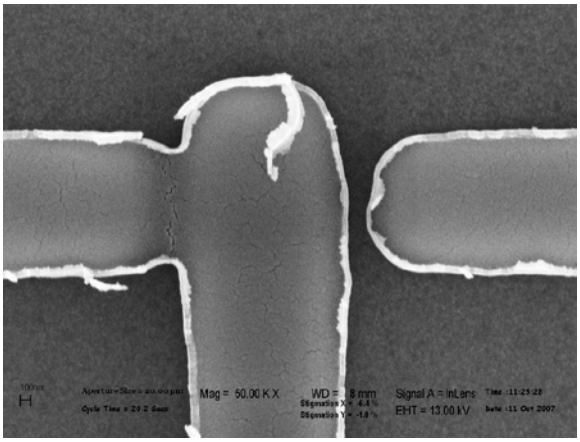

Figure 11 Two electrodes overlapped due to proximity effect.

distance from the area to be exposed, and subtracts the amount of backscattered exposure expected.

Proximity correction algorithms usually describe the scattered beam as a double Gaussian:

$$I = I_0[e^{-\frac{r^2}{2\alpha^2}} + \gamma_E e^{-\frac{r^2}{2\beta^2}}]$$

where α is the proximity parameter for forward scattering, β is the proximity parameter for backward scattering, and γ_E is the ratio of energy deposited due to backscattering to the energy deposited due to the forward scattering.[55] These parameters depend primarily on the resist used, the underlying substrate and most importantly the accelerating voltage. Often these parameters are found by performing Monte Carlo simulations. Once the beam spreading is known the deposited energy at each point can be determined and the dosage map can be adjusted until all points uniformly exposed.

If the feature size is larger than 1 μm, multiple resist layers can be employed to minimize the proximity effect and achieve sharp electrode edges. However, the proximity effect can be used to minimize the face-to-face electrode distances in our case, even though enough empirical data need to be gathered to estimate the line width variation. In layout editing, larger gaps of over 200 nm are designed, but line-width variation caused by the proximity effect will further minimize the actual gaps down below 100 nm.

2.5 Results and discussion

After the nanoswitch fabrication, the samples were treated using oxygen plasma before loaded in the FESEM vacuum chamber for testing. A series of the

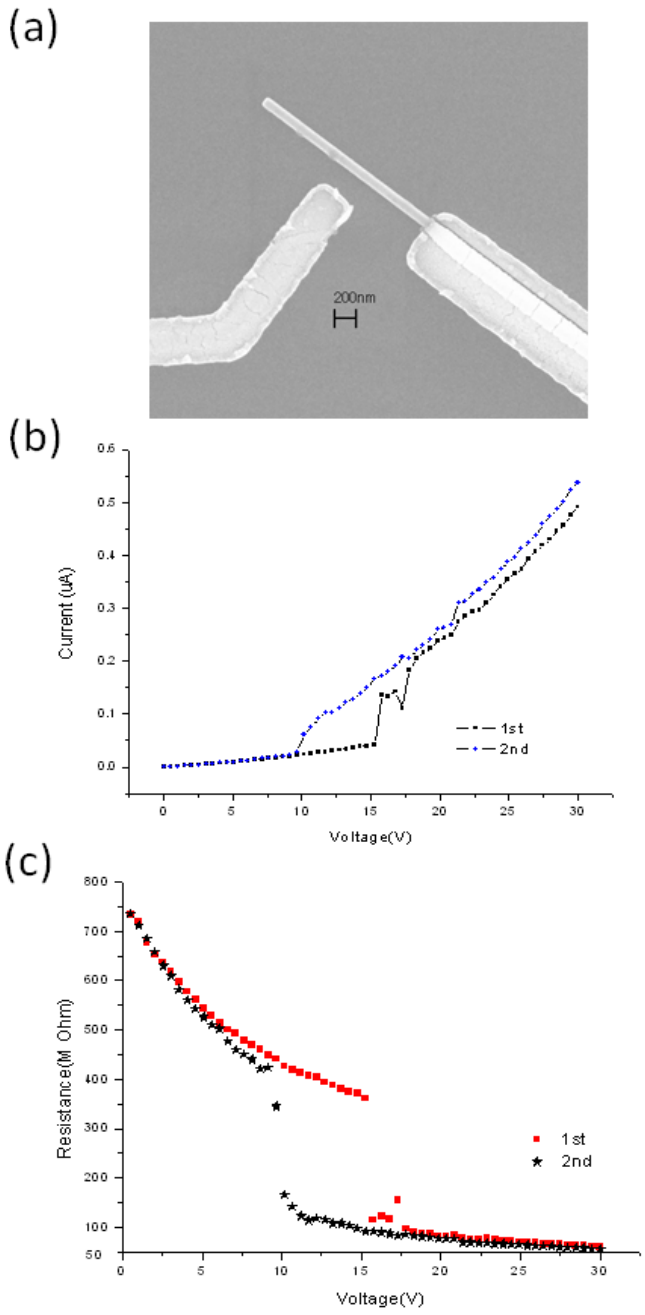

Figure 12 (a) SEM image of a one-way ZnO nanowire nanoswitch (the scale bar is 200nm). (b) *I-V* curve of the nanoswitch. (c) R-V curve of the switch.

electromechanical nanoswitch characterizations were carried out in the vacuum chamber (6×10^{-6} Torr) at room temperature. The test points on the nanoswitches were connected to the electrical probes of the in-chamber micromanipulators, so that the signals can be

sent and received from a computer-controlled Keithley 2400 outside the chamber. Two electrical leads were fabricated for a one-way switch and the electrode suspending the nanowires was connected to the ground while the deflection electrode pulling the end of the nanowire electro-statically was connected to the applied voltage. The voltage was

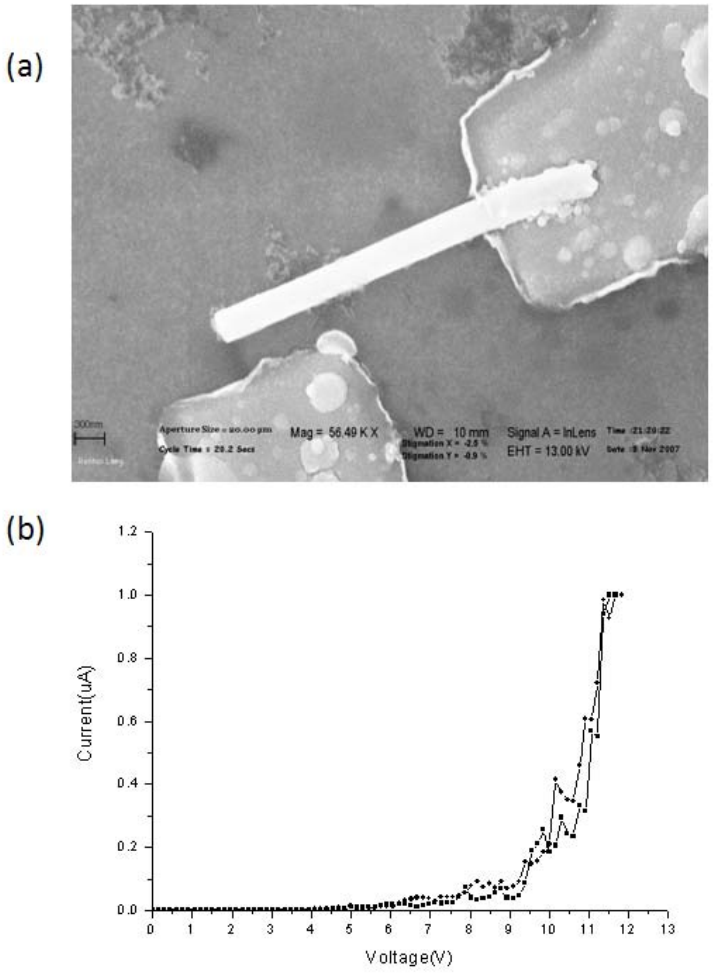

Figure 13(a) SEM image of a one-way Ni nanowire switch (the scale bar is 300nm). (b) *I-V* curve of the nanoswitch.

scanned back and forth from 0 to 10 V, and the currents flowing through the nanowires were also recorded simultaneously. As the bias increased, the accumulated attractive electrostatic force deflected the nanowires toward the facing electrodes to establish an

electrical contact, resulting in a sudden jump of current, namely a sharp drop in the resistance. In Figure 12(a), a 200 nm bending gap in the one-way switch was fabricated using above procedure, where the diameter of the suspended ZnO nanowire is 150 nm. The ON and OFF states of the nanoswitch can be clearly identified from the *I-V* curve in figure 12(b) and *R-V* curve in figure 12(c), respectively. At the OFF state, as the bias voltage increases, the resistance gradually decreases because more electrons can tunnel through the SiO_2 layer or the air under higher bias voltage. At the ON state, the resistance slowly stabilizes as the electrical contact becomes better since the deflected nanowire presses against the electrode much harder at higher bias voltage. Due to the low conductance of our ZnO nanowire, the ON and OFF conductance ratio is about 5:1, as shown in Figure 12(c). It is worth noticing that the turn-on threshold varies since the contact between ZnO nanowire and the electrode can hardly be perfect at the touching moment. In this nanoswitch, the threshold is between 10 V and 15 V. Same method was

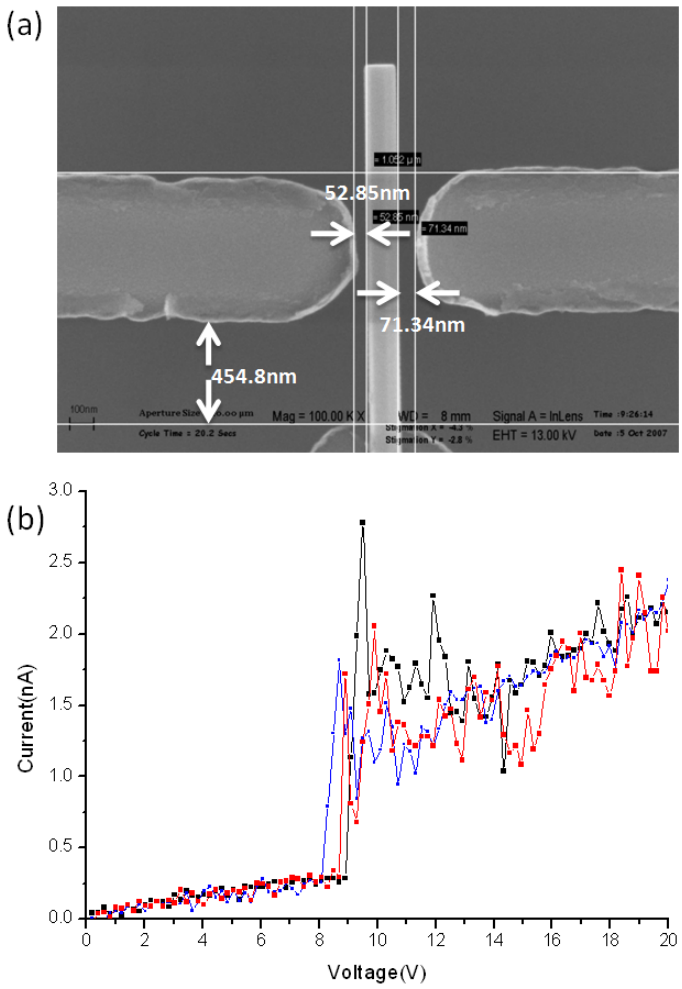

Figure 14 (a) SEM image of a two-way ZnO nanowire nanoswitch (the scale bar is 100nm). (b) *I-V* curve of the left-way nanoswitch.

employed to make a one-way nickel metal nanoswitch, as shown in figure 13(a). The diameter of the nickel nanowire is around 200 nm with suspended length around 2 μm. A bias voltage between 5 V and 7 V could turn on the metal nanoswitch. The rough surface of the electrode causes the slow transition from OFF state to ON state. However, the nickel nanoswitch has better conductance at the ON state which makes leakage current negligible at the OFF state. The ON/OFF conductance ratio of the nickel metal nanoswitch is over 100. A two-way ZnO nanoswitch was also fabricated as shown in figure 14 (a). There was a 10 nm positioning error during *in-situ e*-beam nanolithography process, causing a 10 nm shifting of the both electrodes to the right side and leaving the left gap about 20 nm smaller than the right one. Figure 14 (b) shows the *I-V* measurements of the left way nanoswitch. Since the spacing between the horizontal and the vertical (center) electrode was only about 500 nm, the OFF state leakage current showed kind of big. What made the ON/OFF conductance ratio worse was that the nanowire we patterned had higher resistivity (10Ωcm). Normally, the ZnO nanowire resistivity ranges from 10^{-3} to 10^{5}Ωcm [56].

To rule out the field emission at ON state, a ZnO nanowire patterned as a field emission structure, as shown in figure 15 (a), was fabricated using the similar method. The gap between the tip of the nanowire and the electrode with an applied field is about 200 nm. In the first voltage sweeping, the applied voltage was increased up to 200 V, the emission current was not observed as shown in the blue curve of figure 15 (b). It is necessary to apply a voltage close to 210V to trigger the emission of the nanowires as shown in the red curve of figure 15(b). Based on this result, we can deduce that the emission threshold for a 50 nm gap should be at least over 50 V. Similar experiments on

individual ZnO nanowires were done by Huang Y H *et al.*[57] Therefore, a turn-on voltage

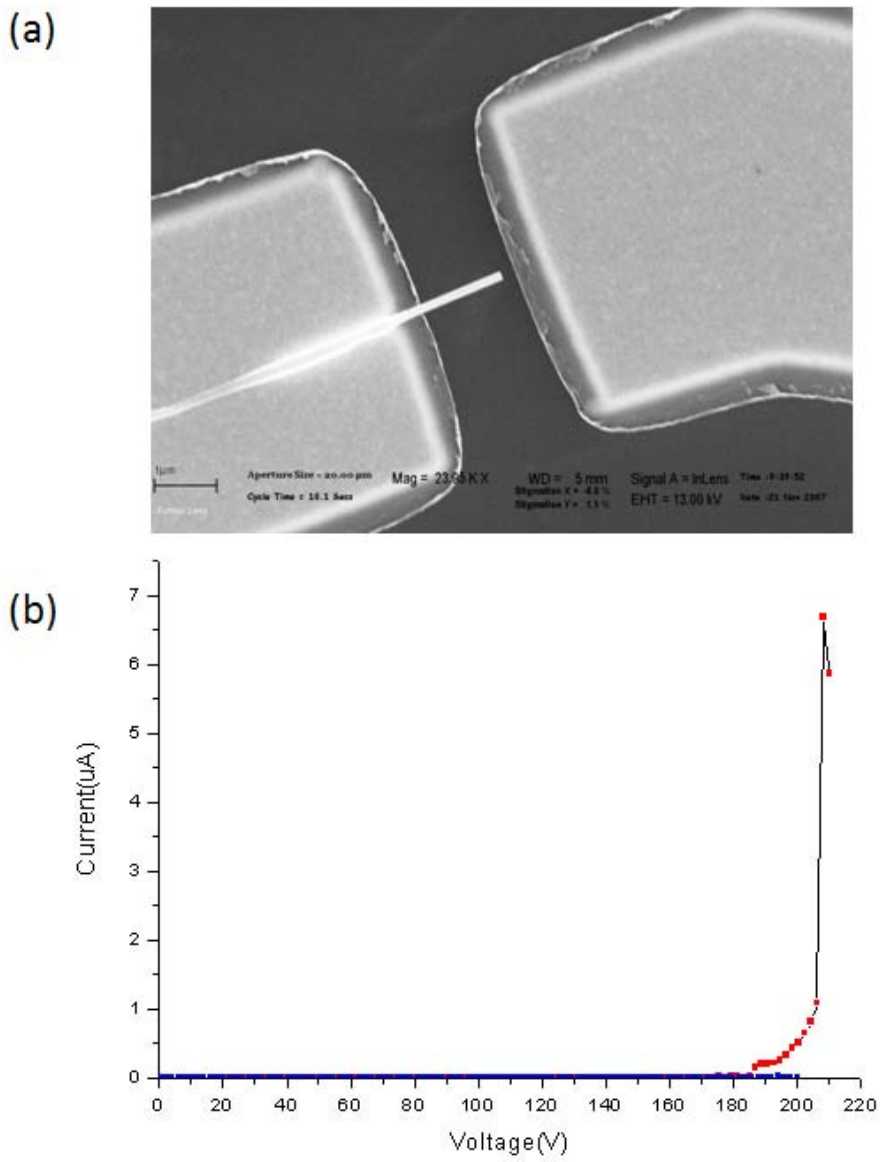

Figure 15 (a) SEM image of a ZnO nanowire field emission structure (the scale bar is 1 μm). (b) Field emission test result of the structure.

of less than 10 V in our nanoswitches can hardly trigger the field emission effect for the suspended ZnO nanowires.

Chapter 3 *In-situ* measurements for one dimensional nano materials characterization

3.1 *In-situ* SEM technology for nano-material characterization

Even though the *in-situ* EBL can easily fabricate many device structures, the small quantity and manual fabrication makes it unfavorable in the exploration stage of understanding the electrical and mechanical properties of the nanomaterials. Meanwhile, the capability to manipulate features in sub-micron range is quite attractive and desirable when the electromechanical property of the materials is unknown. While most of the time SEM is used passively to observe complicated structures at high resolution, a probe system integrated into the SEM chamber can allow us interact with the samples directly. With the capability, some unknown properties of the materials have been discovered[58]. Other than electrical probing and nanomanipulation, *in-situ* SEM can as well be applied in materials science for sample preparation and mechanical characterization.

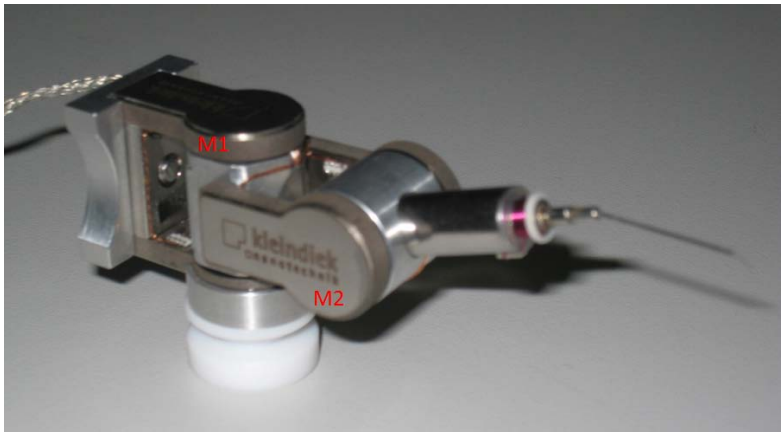

Figure 16 Kleindiek MM3A –EM mircromanipulator

3.2 Tools for *in-situ* SEM nano-material characterization at AMRI

The Kleindiek MM3A –EM mircromanipulator is as shown in figure 16. The movement of the robotic arm is driven by two rotation motors M1 and M2, which control the horizontal and vertical movements, respectively. The third built-in robot controls the in-out movement of the tips, so that the probe tip has 3-freedom movements. Six levels of the movement speed, vibration amplitude and frequency can be configured in the controller (figure 17). The resolution of horizontal, vertical and in-out movement are 5nm, 3.5nm and 0.25nm, respectively. The micromanipulators were fixed to the stage and then screwed to the SEM rotation stage during experiments (figure 18).

Figure 17 Kleindiek MM3A–EM mircromanipulator controller.

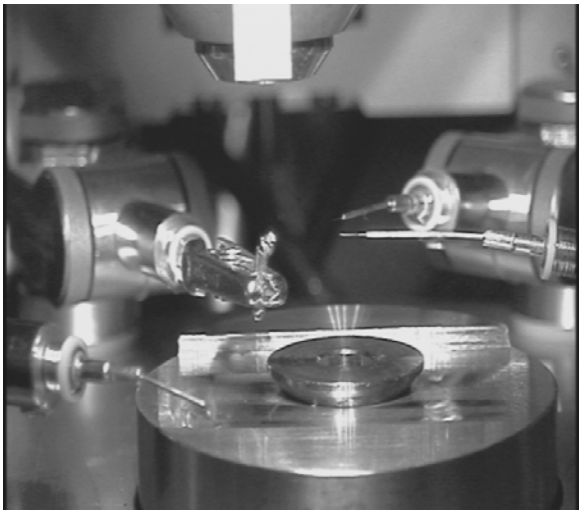

Figure 18 Manipulators installed in SEM chamber.

3.3 Experimental

The *in-situ* manipulation and electrical probing requires proficiency of operation of SEM and correct sample placement. Generally, tip preparation and contact preparation must be done before characterization.

3.3.1 Tip preparation

The probe tips with point radius of 100 nm are tungsten tips provided by the Micromanipulator company (Model: 7X). To remove oxide deposits, the tips need to be dipped into a normal sodium hydroxide (NaOH) solution for a few seconds, then rinsed with deionized water and dried by compressed air. The tips are later heated up or flashed inside the SEM by applying a constant dc current until the contact resistance between the top points of two tips was stabilized below 500 Ω (generally about 10 Ω). Electrochemical etching is the common way to fabricate these tips.

3.3.2 Contact preparation

Generally for objects on solid substrates, good contacts can be made by pressing firmly on the objects. As in figure 18, one probe tip is pressed firmly on the CuO_2 substrate with many CuO_2 nanowires, and the other electrical lead is connected to the substrate using a conducting sample holder. A linear *I-V* curve can easily be retreated without any contact preparation.

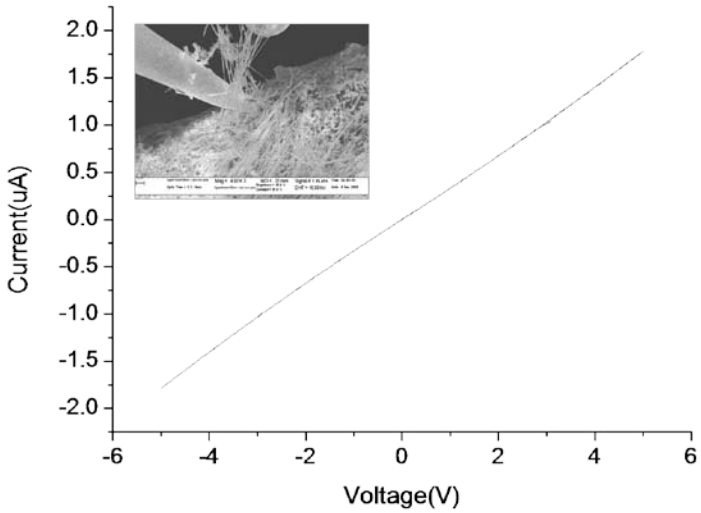

Figure 18 *I-V* characterization of CuO_2 substrate.

However, while probing a single nanowire, the contact is a big issue. In a typical *I-V* characterization, good contacts would produce repeatable results as well as strong

current, while poor contacts resulted in weak signals and large discrepancies between two measurements. However, for suspended nanowires, good contacts need to be made using the Joule heating effect assisted by electron gun bombardment[36]. To demonstrate this approach, three consecutive *I-V* characterization were performed on the sample shown in figure 19 (a). As In figure 19 (b), the first *I-V* curve was measured while the contact was first made. By applying 5 V across the nanowire for a few minutes, the second *I-V* curve was measured, but still there are large mismatches during back and forth voltage sweeping despite of the current increase. The heating continued and later the third *I-V* curve was getting less mismatches and even stronger current. Generally, an almost linear *I-V* curve as shown in figure 20 can be achieved if such routine procedure is kept long enough.

For an *n*-type semiconductor, if the work function of the materials is smaller than the work function of the metal. When contacted, there will be a surface charge region on

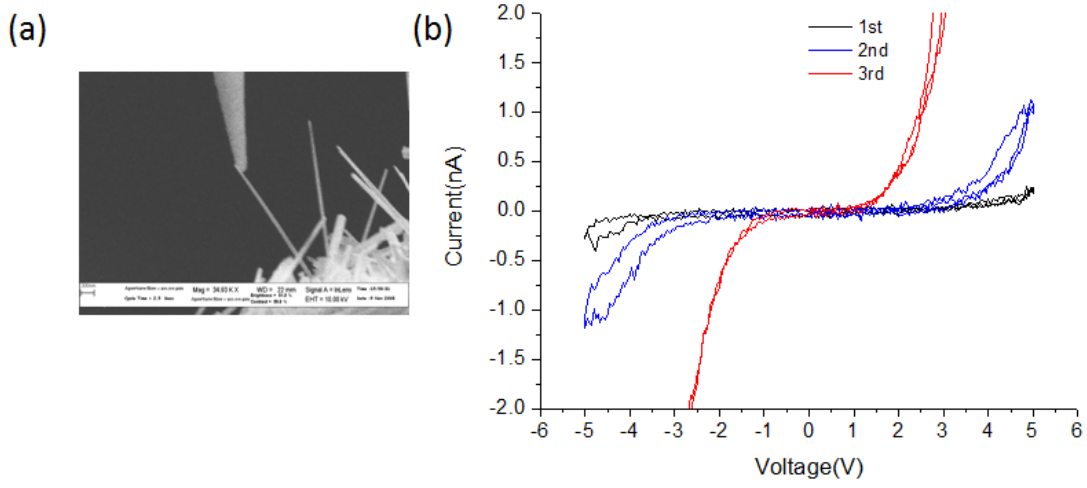

Figure 19 Contact improvement for *in-situ* electrical characterization.

the contact surface of the semiconductor. The electron density in this region is very small, showing high resistance and rectifying effect. However, such a contact barrier is also affected by the surface states density of the semiconductor.

The measured resistance change from GΩ to MΩ for our ZnO nanowires is difficult to understand. Resistance at the interface may be reduced as a result of structure change leading to a larger current across the interface or contact. The contact surface states might change as well, causing lower contact barrier between probe tips and ZnO nanowires. Larger current generates more heat and further lowers the contact resistance. As the contact resistance decreases, the voltage drop at the contact is lower; finally, a balance is achieved and a stable current level is reached. It is not simply a heating effect. A suitable model has not been reported for explaining such phenomenon yet.

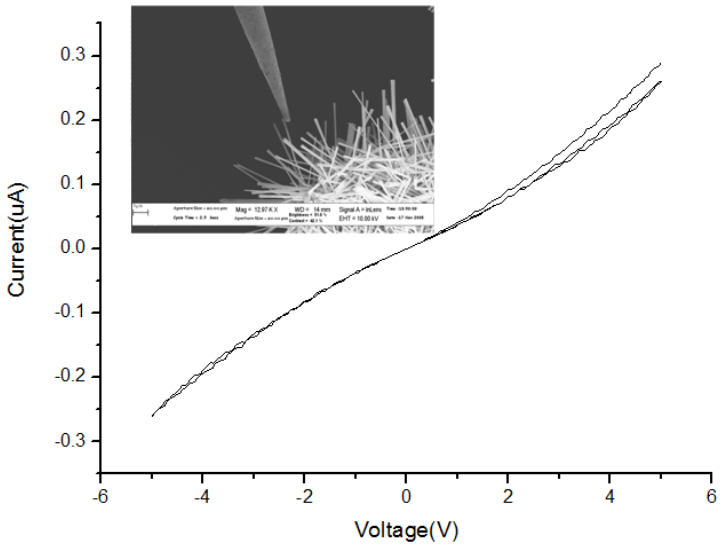

Figure 20 Almost linear *I-V* curve achieved after contact optimization.

3.3.3 Manipulation of objects

Using probe tips for manipulation has many limitations. Generally without large separating force, the tip and objects can be bonded together by Vander Wall force. Such bonding can be improved if the extra current induced heating can melt the joint a little bit. However, in large angle manipulation, electron beam induced deposition of amorphous carbon around the contact area is needed to maintain the contact during nanowire manipulation. Fine step mode should be activated to avoid large abrupt movement of the probe. To have better control over the movement of samples, special tools like grippers, rotating tips and some microscope-compatible adhesive chemicals are necessary.

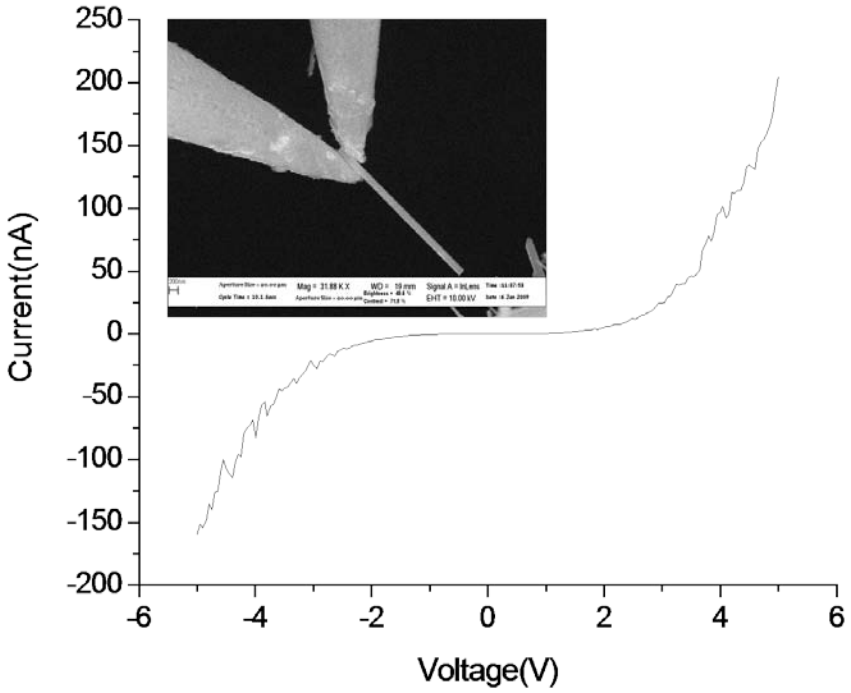

Figure 21 Gripping single ZnO nanowire using two manipulators

3.3.4 *In-situ* gripping and characterization of the cross-section resistance of one-dimensional nano materials

By using two tungsten probe tips at the same time, a single nanowire can be gripped and removed from the nanowire arrays. The first probe tip needs to be moved to the suspended end of the nanowire. By trying to bend the nanowire, it can be told whether the tip and the nanowire are at the same Z level. After that the nanowire can be bent by the first tip, the second probe tip is moved to touch the first tip, so that 2 probe tips and

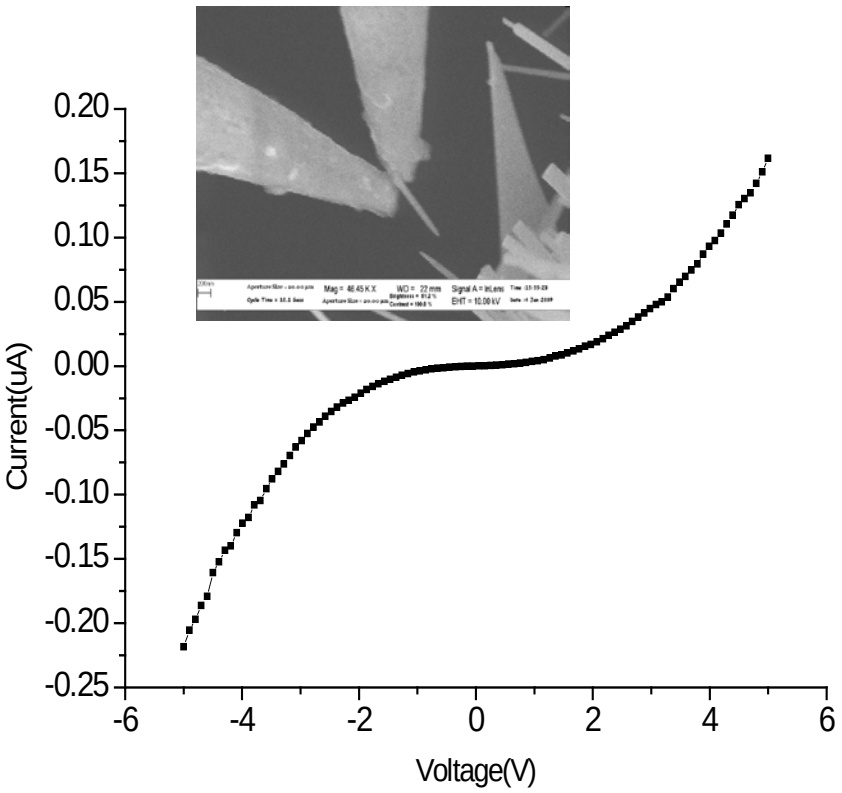

Figure 22 *I-V* characterization of the ZnO nanowire cross section resistance.

the nanowire are at the same Z level. Then, one tip bends the nanowire towards the second tip until the nanowire is sandwiched in between. To separate the nanowire from

the substrate, the substrate is moved away slowly, while the nanowire and the probe tips are kept still. Now that the nanowire is gripped by two probe tips (figure 21), the cross section measurement can be carried out. The contacts still have to be optimized using the routine procedure mentioned above. The *I-V* characterization of the cross-section of the ZnO nanowire shown above is graphed in figure 21. Though the diameter is as small as 150nm, the cross-section resistance is almost as high as that of the longitudinal axis resistance of that nanowire. Another ZnO nanowire as shown in figure 22 shows approximately the same high resistance in cross-section. Such a method might be more suitable for metallic materials measurement rather than the semiconductor measurement as far as the reliability of the metal-semiconductor contact and relatively small spacing between two tips are concerned.

3.3.5 Contact effect study of single ZnO nanowire using *in-situ* electrical characterization

The versatile nanodevices applications by combining the piezoelectric property and the semiconducting property of the ZnO nanowire draw lots of attention recently. On the surface of a deforming nanowire, the potential was non-uniformly distributed due to the piezoelectric effect[59]. That makes it interesting to study how the measurement results of the ZnO nanowire would be affected by the measurement contact points on different locations of the nanowire surface. With the contact points on the stretched side of a deformed ZnO nanowire, *Zhong Lin Wang's* group at Georgia Institute of Technology have demonstrated the concept of piezoelectric gated diodes[60] by bending a single ZnO nanowire. They also first demonstrated the ZnO nanogenerator by changing the contact point from the stretched side to compressed side using an AFM tip[61], which is under heated discussion these days.

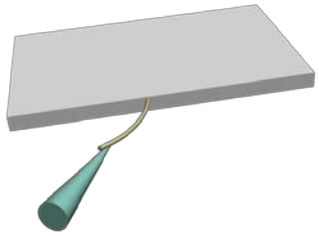

Figure 23 Schematic draw of the probe tip placed on the underside of a ZnO nanowire grown on the aluminum thin foil.

The initial intention was to repeat the nanogenerator experiment using our nano manipulators in SEM. The reversed biased Schottky contact can be easily formed on the stretched side of the nanowire (nanowire has positive potential surface), however, as the tip glides along the surface of the nanowire and reached the compressed point of the nanowire to form the forward biased Schottky contact. No as-reported mV range potential peak can be observed. The experiment can hardly be repeated using our nano

manipulators because: 1) the contact between nanowire and the probe is not reliable enough during movement, which makes it almost impossible to lead charges on the nanowire surface to our nano-voltmeter; 2) the movement of the probe tips and the electron beam can create much noises, whose amplitude can easily exceed 1 mV. Hence, the contact effect is worth studying in advance.

Our study first targeted on the bending induced change of *I-V* curve symmetry of the ZnO nanowire, which was suggested to be the consequence of contact barrier change due to the bending induced piezoelectric potential change. Such phenomenon is supposed to be observed only when the contact point is located on the stretched side of the ZnO nanowire, since a positive potential would be induced on the stretched side to form a barrier between the probe and the nanowire and regulate the current. As the ZnO nanowires are grown on the aluminum thin foil substrate, the ohmic contacts are naturally formed between the nanowire and the substrates. The contact between the probe and nanowire is optimized using our routine Joule heating plus electron gun bombardment procedure[36]. The contact was placed on the underside of ZnO nanowire as schematically shown in figure 23. Such a contact would provide a way for the induced piezoelectric charges cancel themselves in place. Hence, there would be little chance to see the gated diode effect. However, signs of such gated diode effect were found in our experiments.

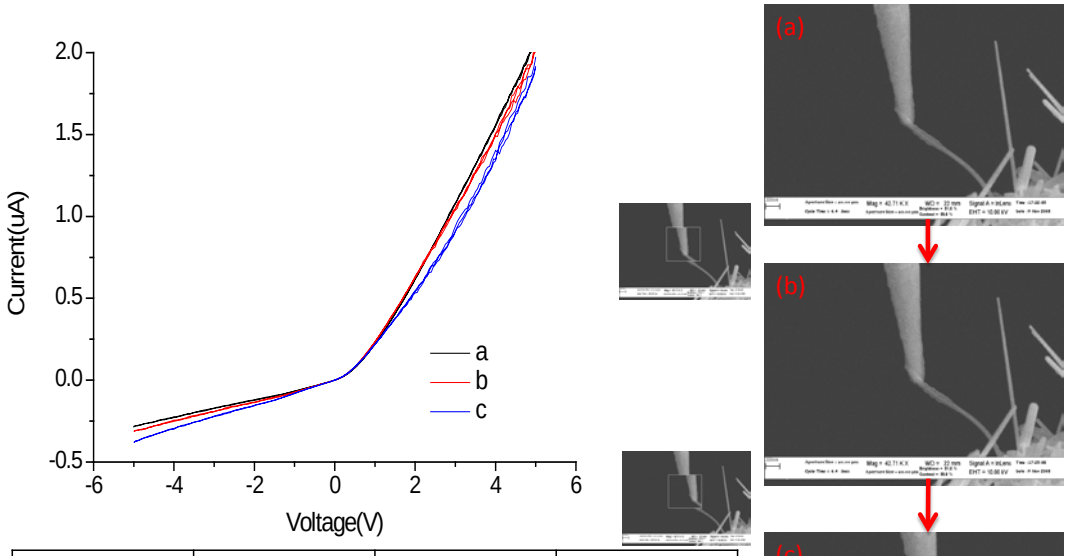

	5V	-5V	Rectifying Ratio
a	2.06uA	-0.284uA	7.25
b	2.03uA	-0.312uA	6.50
c	1.91uA	-0.380uA	5.03

Figure 24 *I-V* characterization of a deformed ZnO nanowire with the contact on the underside. The rectify ratio was decreasing from (a) to (c) when the bending was being reduced.

Electron beam induced deposition of amorphous carbon was used to maintain the contact, so that the tip cannot move on the nanowire surface during the experiment. The nanowire was initially stretched to the right to get the rectifying *I-V* curves. The currents at +5V and -5V are 2.06 μA and -0.284 μA, respectively, showing a rectifying ratio of 7.25:1. Slowly the tip was moved to the right a little bit and the bending would be reduced. Tiny movement step was to make sure the contact point was maintained at the same location. Three *I-V* curves were retrieved as shown in figure 24 and they showed continuous recovering toward symmetry *I-V* curves.

Under the forward biased, the currents across the nanowire were reducing as the stretch to the right was reducing. On the reversed bias part, the currents are increasing as

the bending was being released. The rectifying ratio was reduced from 7.25 to 6.51, then 5.03. The linear *I-V* curve of a straight ZnO nanowire would be changed into a diode-like *I-V* curve under bending. Such gated diode phenomenon was first reported by Z. L. Wang's group on measurements made on the stretched side of the ZnO nanowire[60]. The positive piezoelectric potential induced by bending on the stretched side created a barrier between the stretched surface and the probe, which rectified the current. Here we found that such phenomenon can also be observed when contact was made on the underside.

What's worth mentioning is that the gated diode effect was negligible when the contact points were on the compressed side. The bending was controlled by moving the tip leftward. Even though the bending on the nanowire increased, the bending points actually got away from the contact point, which actually reducing the piezoelectric surface potential around the contact point. That might be the reason why the rectifying ratio steadily decreased from 1.99 to 1.36 then 1.26. The last pulling out movement made the contact point closer to the bending point, which actually increased the rectifying ratio to 1.56 as shown in figure 25. Such changes in rectifying ratio and the rectifying ratio amplitudes are far less noticeable compared to those measured on the underside. Another possible explanation is that the negative surface potential generated by deforming didn't affect the contact barrier where electrons were still able to pass freely in both directions. In that case, there would be no difference in the symmetry of the measured *I-V* curves no matter how hard the nanowire is bent.

Same experiments were also carried out on the stretched sides, but the results are the same with that on the compressed sides. There is another possibility that the as reported gated diode effect is actually a result of the poor contact between nanowire and the probe tips. The paper[60] doesn't report a linear *I-V* curve can be recovered from a

diode-like curve after bending released. More experiments with both the piezoelectric nanowire and non-piezoelectric nanowire should be designed to figure out the mechanism.

As the resistance changes in individual deformed ZnO nanowire have been employed to fabricate sensors[62], it's worth studying such changes. Two things need to be

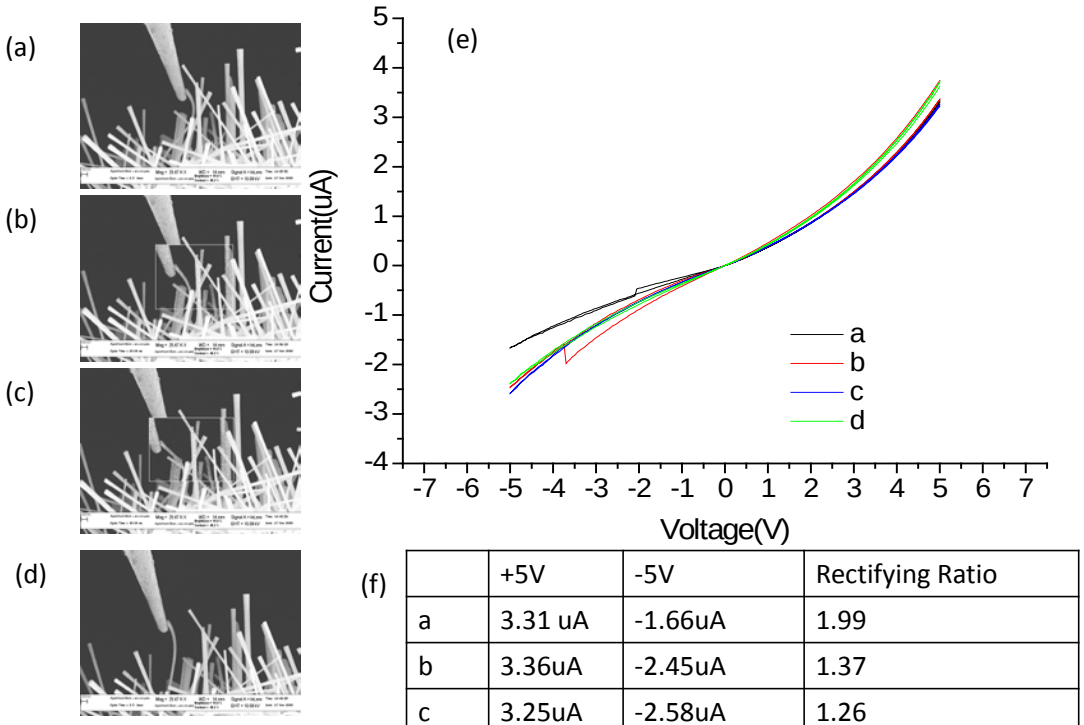

(f)

	+5V	-5V	Rectifying Ratio
a	3.31 uA	-1.66uA	1.99
b	3.36uA	-2.45uA	1.37
c	3.25uA	-2.58uA	1.26
d	3.71uA	-2.38uA	1.56

Figure 25 *I-V* characterization of a deformed ZnO nanowire with the contact on the underside. The rectifying ratio (f) changes are small from (a) to (d) when the bending was being increased.

considered when we compare the resistance changes. One is the contact resistance and the other is the piezoelectric resistance of the nanowire itself. It's hard to study

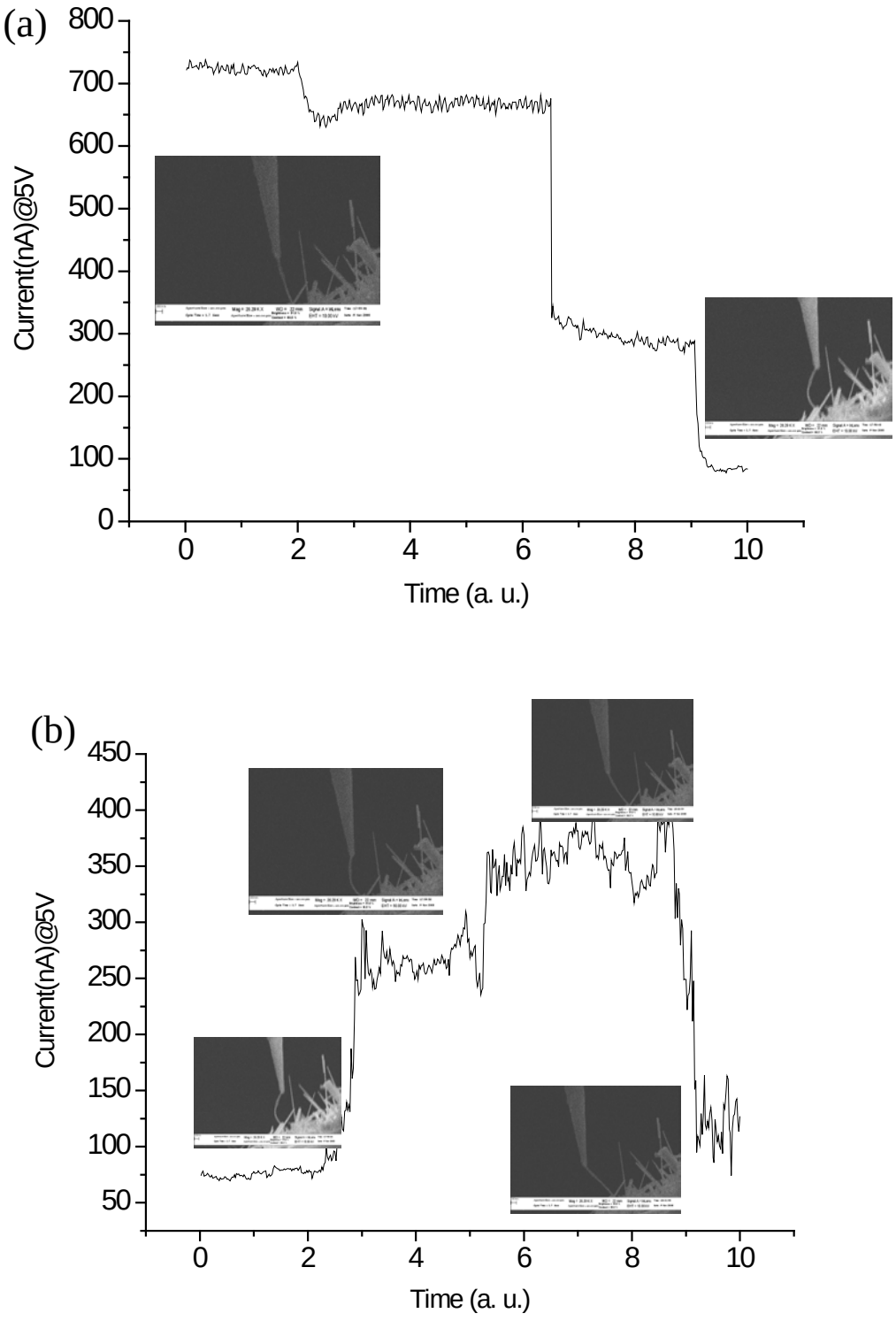

Figure 26 (a) The current dropped as the bending increased. (b)The current recover as the bending was released.

piezoelectric resistance alone without taking any contact resistance changes as the gated diode effect shown above did lead to changes in current under the same bias voltage.

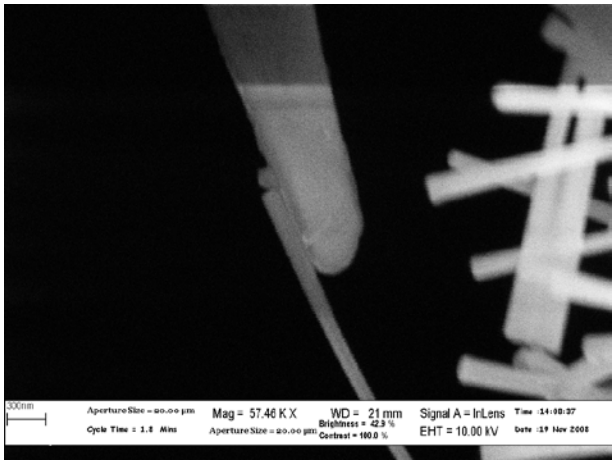

Figure 27 Contact placed on the compressed side of the deformed ZnO nanowire.

To study the piezoelectric resistance changes when contact was made on the underside of the deformed nanowire forward biased at 5V, the nanowire was stretched to the left as shown in figure 26 (a). Slowly the nanowire was moved to the right to increase the bending. Current drops were observed at each movement which increased the stretching to the left. Then again the nanowire was slowly moved to the left (figure 26 (b)), which reduced bending curvature. Current jumps were simultaneously observed at each movement. The last movement which changed the left stretching into right stretching led to large current drops instead of current jumps, which indicated that the contact point might have been moved or the surface polarity of the potential on the contact point might have been changed. The whole experiment showed the measured resistances of the ZnO nanowire were increased as the bending curvature increases, even though it's hard to calculate how much percentage of the increase was contributed by the contact resistance changes. The bending induced resistance changes are also employed to make nano sensors [62,63].

Specifically, a series of characterizations were carried out with the contact point exactly on the compressed side as shown in figure 27. The reversed force of the nanowire,

which was trying to separate the tip and the nanowire, made it easy to form the Schottky contact between the nanowire and the probe. To study the resistance changes with the Schottky contact, the test need to be made with the nanowire forward biased. First, to test the stability of the contact, the tip was moved to the right to increase the compressing. The reversed force of the nanowire became stronger. If the contact point became loose, the current would drop. However, under forward biased, the current across the nanowire increased, which meant the contact point was maintained properly. As the nanowire was released step by step (figure 28), the current dropped accordingly. More compressing on the nanowire induced lower resistance. Less compressing on the nanowire would induce higher resistance. Possibly, the contact barrier was lowered by a negative surface potential rise as the nanowire bending was increased. The last sharp drop was caused by breaking the nanowire. Even though we tried our best to make sure the manipulation of the nanowire would not cause movement of the contact point, the contact resistance might be changed by the surface piezoelectric potential change, which was hard to avoid in such characterizations. The difficulties in eliminating the contact effect in our characterization made it hard for us to study relationship between the piezoresistance and the bending curvature. Still, another possible explanation is that the ZnO nanowires under study have different polarizations[64] and behave differently under bending.

Since the results in figure 24 show behaviors which are close to those of the Schottky contacts. We assume that the changes are mainly from the barrier height changes caused by piezoelectricity. According to the thermionic emission theory, the following equation can describe the *I-V* characteristics of the tested nanowire under bending:

$$I_s = Ae^{-\varphi_{pz}/kT}(e^{-qv/kT} - 1)$$

where φ_{pz} is the potential energy barrier resulting from piezoelectricity, I_s is the reverse saturation current, V is the applied voltage, q is the electron charge, k is the Boltzmann constant 8.617×10^{-5}eVKK^{-1}), T is the absolute temperature, and A is a constant[60]. We consider the current at -5V and room temperature with different bending degrees. With 0 degree bending degree, the current is assumed to be the same as that at +5V, which is about 2 μA for nanowire in figure 24. In addition, at 0 degree bending, the piezoelectric potential is zero, i.e. $\varphi_{pz} = 0$. Then, we can get $I_{s0} = Ae^{-\frac{\varphi_{pz}}{kT}}\left(e^{-\frac{qv}{kT}} - 1\right) = A\left(e^{-\frac{qv}{kT}} - 1\right) = 2\mu A.$

At condition a of figure 24, $I_{sa} = I_{s0}e^{-\frac{\varphi_{pz}}{kT}} = 2\mu A \times e^{-\frac{\varphi_{pz}}{kT}} = 0.284\mu A,$ which gives φ_{pz}=0.0505eV. In the same way, we get the piezoelectric potential energy barrier reduced to 0.048eV and 0.0429eV for condition b and c, respectively.

For the *I-V* curves in figure 28 (a), a Metal-Semiconductor-Metal model[65] is used to estimate the barrier change. At the initial bending, the contact barrier is estimated to be 0.595 eV, and lowered to 0.584 eV as more bending gets the compressed surface more negatively charged.

The bending induced resistance increases are also found by *in-situ* transmission microscopy[66,67]. In many of our *in-situ* experiments, no resistance changes by bending were observed if the contacts hadn't been optimized till the current through the nanowire show signs of saturation. Since the identification and elimination of artifacts are challenging, further efforts should be made to understand the mechanisms.

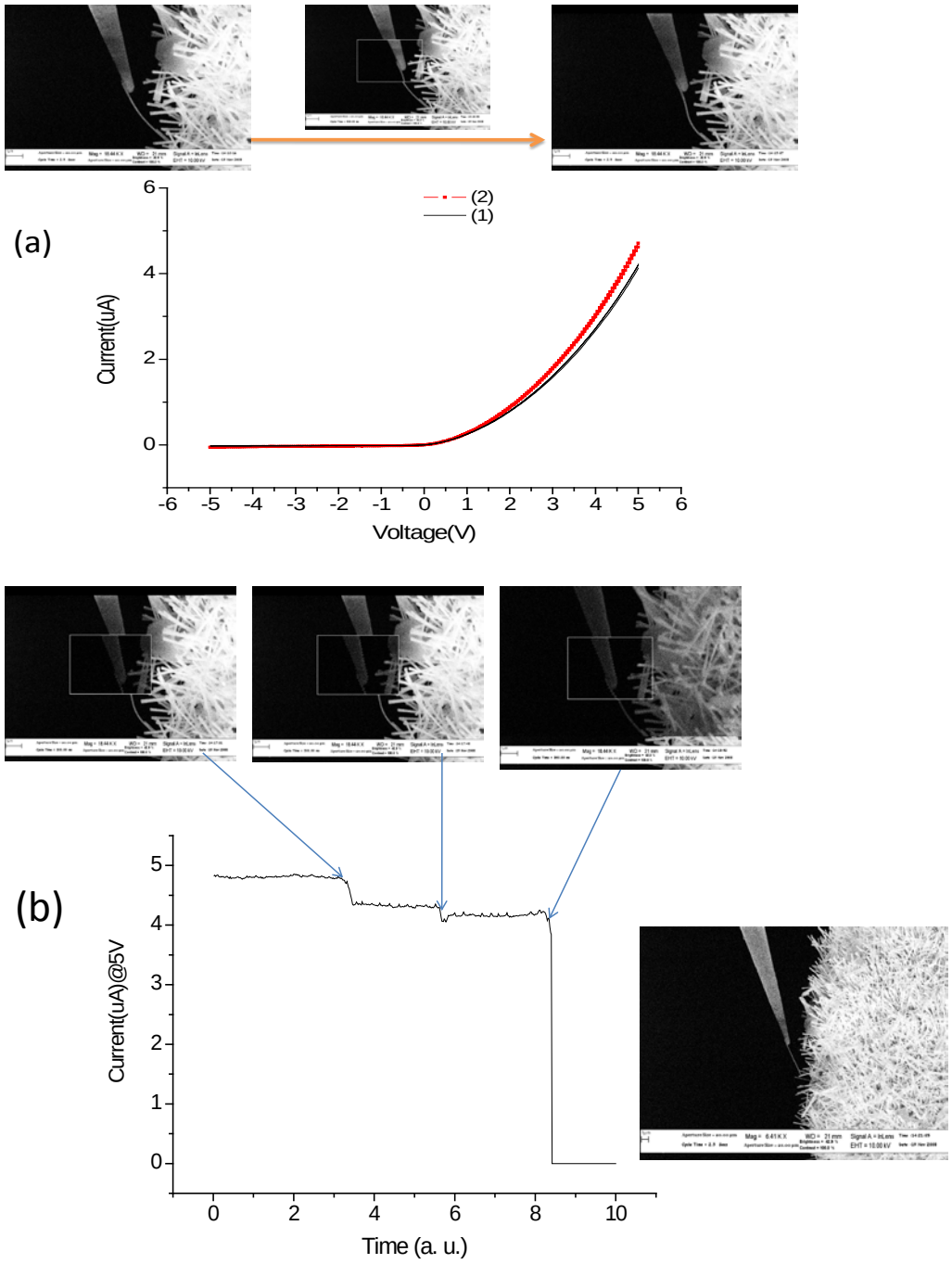

Figure 28 (a) Test reliability of the contact on the compressed side by increasing the bending. (b) Current decreases as the bending is being reduced.

Chapter 4 Conclusion

In conclusion, we demonstrate a precise voltage-contrast image aided positioning during *in-situ e*-beam nanolithography through the fabrication of suspended nanowire based nanoswitches. The method of sandwiching the nanowires between two layers of photoresist effectively simplifies the fabrication process of the suspended structure. The positioning error can be reduced to 10 nm in our fabrication, which is sufficient for most NEMS fabrications. Details on using rapid voltage-contrast imaging to register the location of the nanowires without exposing the photoresist have been discussed. Layout editing for positioning optimization has also been covered. The measurements on different nanoswitches in the FESEM vacuum chamber present well-defined ON and OFF states induced by changing the applied voltages, which also proves the reliability of as-demonstrated process. This simplified process provides an easy, low cost and less time consuming route to integrate suspended nanowire based structures using a converted FESEM *e*-beam system, which can also be customized to fabricate multi-layer structures for nanodevice applications.

The *in-situ* measurements using manipulators in SEM has been demonstrated to study the ZnO piezoelectronics, which is under heated discussion. Our *in-situ* measurements of the ZnO nanowire show that the contacts affect the measurements, which might be the reason that the results are not consistent. Special attentions need to be paid to the contact effects as well as the identification and elimination of artifacts.

References

[1] L. A. W. Robinson, S. B. Lee, K. B. K. Teo, M. Chhowalla, G. A. J. Amaratunga, W. I. Milne, D. A. Williams, D. G. Hasko, and H. Ahmed, NANOTECHNOLOGY**,** 290-293 (2003).

[2] R. Long, J. Chen, J. Lim, Y. Yao , J. Wiley and W. Zhou (accepted by Nanotechnology for publication, 2009).

[3] R. Long, K. Wang, J. Chen, and W. Zhou (Preparing for submission).

[4] M. S. Bobji, J. B. Pethica, and B. J. Inkson, Journal of Materials Research **20,** 2726-2732 (2005).

[5] X. G. Ma and K. Komvopoulos, Journal of Materials Research **20,** 1808-1813 (2005).

[6] A. M. Minor, E. T. Lilleodden, E. A. Stach, and J. W. Morris, in *In-situ transmission electron microscopy study of the nanoindentation behavior of Al*, 2002 (Minerals Metals Materials Soc), p. 958-964.

[7] T. Ohmura, A. Minor, K. Tsuzaki, and J. W. Morris, in *Indentation-induced deformation behavior in martensitic steel observed through in-situ nanoindentation in a transmission electron microscopy*, 2006 (Trans Tech Publications Ltd), p. 239-244.

[8] J. S. Robach, I. M. Robertson, B. D. Wirth, and A. Arsenlis, Philosophical Magazine **83,** 955-967 (2003).

[9] F. Delmas, M. Vivas, P. Lours, M. J. Casanove, A. Couret, and A. Coujou, Materials Science and Engineering a-Structural Materials Properties Microstructure and Processing **340,** 286-291 (2003).

[10] D. Baither, T. Krol, and E. Nembach, in *Dislocation processes in precipitate-free zones in NIMONIC PE16 studied by in situ transmission electron microscopy*, 2004 (Elsevier Science Sa), p. 163-166.

[11] K. Hattar, J. Han, M. T. A. Saif, and I. M. Robertson, Journal of Materials Research **20,** 1869-1877 (2005).

[12] S. G. Pyo and N. J. Kim, Journal of Materials Research **20,** 1888-1901 (2005).

[13] A. Kroger, R. Wernhardt, C. Somsen, G. Eggeler, and A. Wieck, in *In situ transmission electron microscopy-investigations on the strain-induced B19 '-phase in NiTi shape memory alloys structured by focused ion beam*, 2006 (Elsevier Science Sa), p. 513-516.

[14] J. Olbricht, M. F. X. Wagner, A. Condo, A. Dlouhy, C. Grossmann, A. Kroger, C. Somsen, and G. Eggeler, International Journal of Materials Research **99,** 1150-1156 (2008).

[15] N. Zarubova, J. Gemperlova, V. Gartnerova, and A. Gemperle, in *Stress-induced martensitic transformations in a Cu-Al-Ni shape memory alloy studied by in situ transmission electron microscopy*, 2008 (Elsevier Science Sa), p. 457-461.

[16] T. Sumitomo, H. Kakisawa, Y. Owaki, and Y. Kagawa, Journal of Materials Research **23,** 1466-1471 (2008).

[17] D. Baither, V. Mottles, and E. Nembach, Journal of Materials Research **20,** 1722-1727 (2005).

[18] N. Zarubova, A. Gemperle, and J. Gemperlova, in *Local stress modification during in situ transmission electron microscopy straining experiments*, 2007 (Elsevier Science Sa), p. 407-411.

[19] H. S. Tang, T. J. Hermel-Davidock, S. F. Hahn, D. J. Murray, R. C. Cieslinski, N. E. Verghese, and H. Q. Pham, Journal of Polymer Science Part B-Polymer Physics **47,** 393-406 (2009).
[20] A. Nafari, D. Karlen, C. Rusu, K. Svensson, H. Olin, and P. Enoksson, Journal of Microelectromechanical Systems **17,** 328-333 (2008).
[21] T. Y. Kim, S. W. Kim, E. Olson, and H. M. Zuo, Ultramicroscopy **108,** 613-618 (2008).
[22] M. A. Verheijen, J. Donkers, J. F. P. Thomassen, J. J. van den Broek, R. A. F. van der Rijt, M. J. J. Dona, and C. M. Smit, Review of Scientific Instruments **75,** 426-429 (2004).
[23] J. C. Bennett, C. V. Hyatt, M. A. Gharghouri, S. Farrell, M. Robertson, J. Chen, and G. Pirge, in *In situ transmission electron microscopy studies of directionally solidified Ni-Mn-Ga ferromagnetic shape memory alloys*, 2004 (Elsevier Science Sa), p. 409-414.
[24] J. Cumings, E. Olsson, A. K. Petford-Long, and Y. M. Zhu, Mrs Bulletin **33,** 101-106 (2008).
[25] C. Q. Chen, Y. Shi, Y. S. Zhang, J. Zhu, and Y. J. Yan, Physical Review Letters **96** (2006).
[26] D. Stickler, R. Fromter, W. Li, A. Kobs, and H. P. Oepen, Review of Scientific Instruments **79** (2008).
[27] M. D. Halliday, P. Poole, and P. Bowen, Fatigue & Fracture of Engineering Materials & Structures **18,** 717-729 (1995).
[28] A. Poursartip, A. Gambone, S. Ferguson, and G. Fernlund, Engineering Fracture Mechanics **60,** 173-185 (1998).
[29] A. A. Yawny and J. E. P. Ipina, Journal of Testing and Evaluation **31,** 413-422 (2003).
[30] R. Rizzieri, F. S. Baker, and A. M. Donald, Review of Scientific Instruments **74,** 4423-4428 (2003).
[31] Y. Zhu, N. Moldovan, and H. D. Espinosa, Applied Physics Letters **86,** 3 (2005).
[32] C. J. Boehlert, C. J. Cowen, S. Tamirisakandala, D. J. McEldowney, and D. B. Miracle, Scripta Materialia **55,** 465-468 (2006).
[33] S. B. Hosseini, C. Temmel, B. Karlsson, and N. G. Ingesten, Metallurgical and Materials Transactions a-Physical Metallurgy and Materials Science **38A,** 982-989 (2007).
[34] K. I. Dragnevski, T. W. Fairhead, R. Balsod, and A. M. Donald, Review of Scientific Instruments **79,** 3 (2008).
[35] W. M. Xiao, Y. W. Shi, Y. P. Lei, Z. D. Xia, and F. Guo, Journal of Electronic Materials **37,** 1751-1755 (2008).
[36] Q. Chen, S. Wang, and L. M. Peng, Nanotechnology **17,** 1087-1098 (2006).
[37] C. H. Ke and H. D. Espinosa, Small **2,** 1484-1489 (2006).
[38] F. Bussolotti, L. D'Ortenzi, V. Grossi, L. Lozzi, S. Santucci, and M. Passacantando, Physical Review B **76,** 7 (2007).
[39] S. A. Campbel, *Fabrication Engineering at the Micro and Nanoscale*, 3 ed. (Oxford University Press, USA, 2007).
[40] M. A. McCord and M. J. Rooks, in *SPIE Handbook of Microlithography, Micromachining and Microfabrication*; *Vol. 1*, edited by P. Rai-Choudhury (SPIE Publications, 1997).

[41] L. A. C. Joe Nabity, Mo Zhu and Weilie Zhou, in *Scanning Microscopy for NanotechnologyTechniques and Applications* (Springer New York, 2007).
[42] X. L. Feng, R. R. He, P. D. Yang, and M. L. Roukes, Nano Letters **7,** 1953-1959 (2007).
[43] R. R. He, X. L. Feng, M. L. Roukes, and P. D. Yang, Nano Letters **8,** 1756-1761 (2008).
[44] G. S. Snider and R. S. Williams, Nanotechnology **18** (2007).
[45] X. F. Duan, Y. Huang, R. Agarwal, and C. M. Lieber, Nature **421,** 241-245 (2003).
[46] D. Whang, S. Jin, Y. Wu, and C. M. Lieber, Nano Letters **3,** 1255-1259 (2003).
[47] V. Sazonova, Y. Yaish, H. Ustunel, D. Roundy, T. A. Arias, and P. L. McEuen, Nature **431,** 284-287 (2004).
[48] H. Takemura, H. Ohki, H. Nakazawa, Y. Nakagawa, M. Isobe, Y. Ochiai, T. Ogura, M. Narihiro, and T. Mogami, in *Performance of new E-beam lithography system JBX-9300FS*, 2000 (Elsevier Science Bv), p. 329-332.
[49] Y. C. Lin and T. E. Everhart, Journal of Vacuum Science & Technology **16,** 1856-1860 (1979).
[50] T. Brintlinger, Y. F. Chen, T. Durkop, E. Cobas, M. S. Fuhrer, J. D. Barry, and J. Melngailis, Applied Physics Letters **81,** 2454-2456 (2002).
[51] T. Nakasugi, A. Ando, K. Sugihara, Y. Yamazaki, M. Miyoshi, and K. Okumura, JOURNAL OF VACUUM SCIENCE & TECHNOLOGY B**,** 2869-2873 (2001).
[52] K. Y. Lee, Y. Hsu, P. Le, Z. C. H. Tan, T. H. P. Chang, and K. Elian, in *1 kV resist technology for microcolumn-based electron-beam lithography*, 2000 (Amer Inst Physics), p. 3408-3413.
[53] T. Nakasugi, A. Ando, K. Sugihara, M. Miyoshi, and K. Okumura, Proceedings of SPIE **4343,** 334 (2001).
[54] J. P. Vigouroux, J. P. Duraud, A. Lemoel, C. Legressus, and D. L. Griscom, Journal of Applied Physics **57,** 5139-5144 (1985).
[55] T. H. P. C. a. A. D. G. Stewart, Electron-Beam, X-Ray, and Ion-Beam Submicrometer Lithographies (1969).
[56] E. Schlenker, A. Bakin, T. Weimann, P. Hinze, D. H. Weber, A. Golzhauser, H. H. Wehmann, and A. Waag, Nanotechnology **19,** 7 (2008).
[57] Y. H. Huang, X. D. Bai, Y. Zhang, J. J. Qi, Y. S. Gu, and Q. L. Liao, Journal of Physics-Condensed Matter **19,** 7 (2007).
[58] Q. S. Zheng, B. Jiang, S. P. Liu, Y. X. Weng, L. Lu, Q. K. Xue, J. Zhu, Q. Jiang, S. Wang, and L. M. Peng, Physical Review Letters **100** (2008).
[59] Y. Gao and Z. L. Wang, Nano Letters **7,** 2499-2505 (2007).
[60] J. H. He, C. L. Hsin, J. Liu, L. J. Chen, and Z. L. Wang, Advanced Materials **19,** 781-+ (2007).
[61] Z. L. Wang and J. H. Song, Science **312,** 242-246 (2006).
[62] X. D. Wang, J. Zhou, J. H. Song, J. Liu, N. S. Xu, and Z. L. Wang, Nano Letters **6,** 2768-2772 (2006).
[63] J. Zhou, Y. D. Gu, P. Fei, W. J. Mai, Y. F. Gao, R. S. Yang, G. Bao, and Z. L. Wang, Nano Letters **8,** 3035-3040 (2008).
[64] Y. Li, Q. F. Xing, Y. Yan, and W. L. Zhou, Journal of Nanoscience and Nanotechnology (2009).

[65] Z. Y. Zhang, K. Yao, Y. Liu, C. H. Jin, X. L. Liang, Q. Chen, and L. M. Peng, Advanced Functional Materials **17,** 2478-2489 (2007).
[66] P. Gao, Z. Z. Wang, K. H. Liu, Z. Xu, W. L. Wang, X. D. Bai, and E. G. Wang, Journal of Materials Chemistry **19,** 1002-1005 (2009).
[67] K. H. Liu, P. Gao, Z. Xu, X. D. Bai, and E. G. Wang, Applied Physics Letters **92** (2008).

Vita

Renhai Long was born in Zhanjiang city, China, on September 24, 1984, the son of Kangshou Long and Yan Li. In September 2002, he went to Sichuan University where he studied microelectronics and received his Bachelor of Science in June 2006. In August 2006, he moved to New Orleans and entered The Graduate School at The University of New Orleans.